MJFAS
Malaysian Journal of Fundamental and Applied Sciences

Mangsor *et al.* | Malaysian Journal of Fundamental and Applied Sciences, Vol. 20 (2024) 939–945

RESEARCH ARTICLE

Melt Pool Flow Dynamics of Copper Imbued Surface Alloyed 304 Stainless Steel: Role of Laser Power and Scanning Speed Tuning

A. S. Mangsor[a,b], A. A. Salim[a,b], S. K. Ghoshal[a,b], M. S. Aziz[a,b*]

[a]Laser Center, Ibnu Sina Institute for Scientific and Industrial Research, Universiti Teknologi Malaysia, 81310 UTM Johor Bahru, Johor, Malaysia; [b]Department of Physics, Faculty of Science, Universiti Teknologi Malaysia, 81310 UTM Johor Bahru, Johor, Malaysia

Abstract This study emphasizes the crucial role of Marangoni convection in the laser surface-alloying of 304 stainless steel (304 SS) with copper (Cu). By studying the microscopic behavior of the melt pool during CO_2 laser alloying, the study reveals the association between Marangoni convection and the resulting microstructure. The findings demonstrate that the most optimum deposited track can be observed at power 80 W with a scanning speed of 0.4950 mm/s while the highest scanning speed of 0.6329 mm/s produced the finest grains. From the microhardness analysis, sample with the scanning speed of 0.6329 mm/s yielded the best microhardness due to fast cooling and solidification, highlighting the importance of controlling the process parameters to achieve the desired outcome. This data provides valuable insights into the laser-matter interaction and underscores the need to understand underlying melt pool flow dynamics mechanisms such as Marangoni convection to optimize the process for high-quality results.

Keywords: Laser surface alloying, melt pool dynamics, 304 stainless steel, copper.

Introduction

The Laser surface alloying (LSA) is a thermo-chemical procedure that uses high-energy laser beams to modify the surface composition of materials, enhancing their properties without altering the bulk structure [1]. This process involves melting a pre-applied or co-applied metal coatings on a substrate to create an alloyed with improved wear resistance, corrosion resistance, and mechanical strength. With applications ranging from automotive parts to aerospace components, laser surface alloying is paving the way for lighter, stronger, and more durable materials in various industries. Previously, the utilization of continuous wave (CW) laser commonly CO_2 has been reported in the majority of LSA work due to its homogenous surface process, larger surface coverage and deeper melt-depth penetration [2-5].

In the context of melt pool flow dynamics during LSA, the forces acting on the fluid flow, including buoyancy force, Marangoni force, gravity, and shear force, have been studied [6-8]. Interestingly, previous research has highlighted the dominance of the Marangoni force in influencing heat transfer, solidification behavior and defects formation [9]. Figure 1 illustrates the Marangoni convection during laser surface alloying process. Uneven heating during laser beam irradiation leads to temperature variations, with the center of the melt pool experiencing the highest temperature and radial temperature decrease. This temperature gradient induces a surface tension difference in the melt pool, resulting in an outward melt flow driven by the Marangoni force. Previously, research has focused on integrating the understanding of melt pool dynamics with LSA processes to optimize alloying parameters and enhance the quality of surface-modified materials. By coupling computational fluid dynamics (CFD) simulations with experimental observations, researchers have aimed to predict and control melt pool behavior during LSA, leading to improved process efficiency and alloyed surface quality [10-12]. However, there are still challenges in accurately modeling and predicting the complex interactions between laser energy, material properties, and melt pool dynamics during LSA. Further experimental work is needed to explore approaches for optimizing process parameters, enhancing alloying efficiency, and ensuring the reproducibility and reliability of surface modification using LSA techniques.

***For correspondence:**
safwanaziz@utm.my

Received: 01 Feb. 2024
Accepted: 19 April 2024

In this study, Cu has been chosen as the coating additive for 304 SS in LSA. SS is widely used in industrial applications due to its corrosion resistance, mechanical properties, and cost-effectiveness, but it suffers from poor hardness and wear resistance [13-15]. By introducing Cu as an alloying element, we aim to elevate the performance of austenitic stainless steel. Theoretical considerations suggest that Cu, being immiscible with Fe and Cr (the main components of the substrate) in the liquid states, holds potential in this context [16-17].

In summary, this work is important as it addresses the limitations of 304 SS and explores the potential of Cu as an alloying element through LSA. The investigation of process parameters and their relation with melt pool flow dynamics highlight the new perspectives and advancements offered by this research. These results will contribute to expanding the knowledge and applications of laser surface alloying, ultimately leading to improved surface properties and performance in various industrial settings.

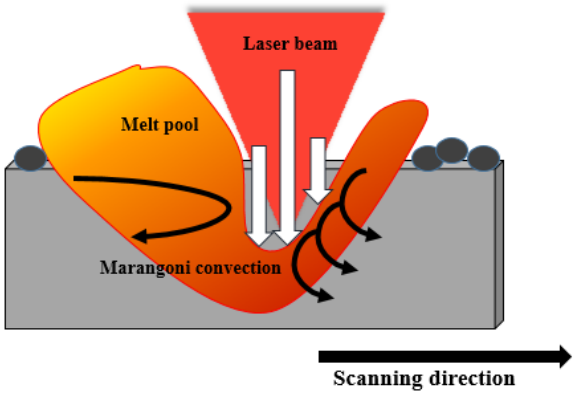

Figure 1. Illustration of Marangoni convection during laser surface alloying process

Materials and Methods

The substrates used in this experiment were 304 SS with dimensions of 1 x 1 x 0.3 cm. The alloying additive used in the experiment was pure copper powder. Surface of 304SS substrate was cleaned thoroughly using citric acid solution to remove any contaminants such as grease, oil, rust or dirt. The substrate was then went through preheating under at temperature 150°C at 30 minutes to improve the adhesion of the coating by reducing thermal stresses and promoting interfacial bonding between the substrate and sprayed material. To start the coating process, 304 SS surface (99%) was painted with 20 wt/% polyvinyl alcohol (PVA) solution prior to spraying it with the alloying element via spray coating process. The arc spraying gun was moved systematically across the substrate surface to achieve uniform coverage and the desires coating thickness. The coated samples were then left to dry inside an oven set at 90° C for 1 hour. Thickness of the powder coating produced was maintained at 0.2 mm throughout the experiment.

Laser Surface Alloying (LSA)

Figure 2 shows the experimental setup for LSA in (a) laser surface alloying system and (b) schematic diagram of laser alloying. The sprayed coated substrates were melted using a CW CO_2 laser at the maximum power of 80 W with a laser beam spot size of 3 mm and 15 cm stand-off distance. Simultaneously, the moving stage holding the sample moved in a horizontal direction allowing the melting of the powder and substrate thus forming an alloyed track. The melting process was conducted in an enclosed container with a constant flow of argon gas at 20 sccm directed into the generated molten pool during LSA to prevent contamination and oxidation to the deposited sample. In this study, two laser parameters were varied including power P (W) and scanning speed v (mm/s) to investigate their effect on microstructural and surface hardness properties of the melt pool and deposited track of laser surface-alloyed. The morphological properties of the deposited track was examined by Scanning Electron Microscope (SEM, JOEL) while microhardness was obtained from the Vickers microhardness test. For samples with varying power from 55 W to 80 W, the scanning speed was maintained at 0.4950 mm/s

with indentation time of 10 s and indent force of 500 gf. Meanwhile, for samples with varying scanning speed from 0.4132 mm/s to 0.6329 mm/s, the laser power was fixed at 75 W with indentation time of 10 s and indent force of 500 gf.

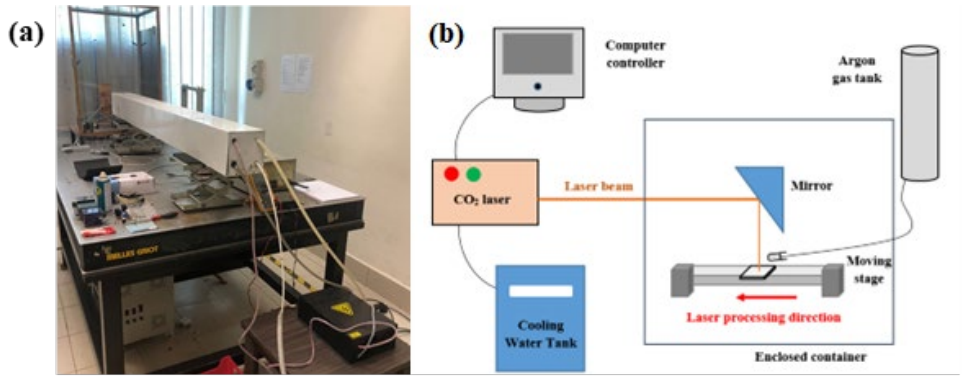

Figure 2. Experimental setup for LSA in (a) laser surface alloying system and (b) schematic diagram of laser alloying

Results and Discussion

Figure 3 (a, b) shows the Cu powder surface morphology and EDX spectra of the deposited track 304 SS. The particle size was measured and determined at the range between 275.11 nm to 494.60 nm. The particles observed were in spherical shape, exactly the shape needed for maximum powder bed density that would lead to high density and flowability of the alloyed parts [18, 19]. Fe, Cr, Ni, C and Al peaks were observed indicating the elements presented in the 304 SS. A small percentage of Al can be classified as impurities (Figure 3 (b)).

(a)

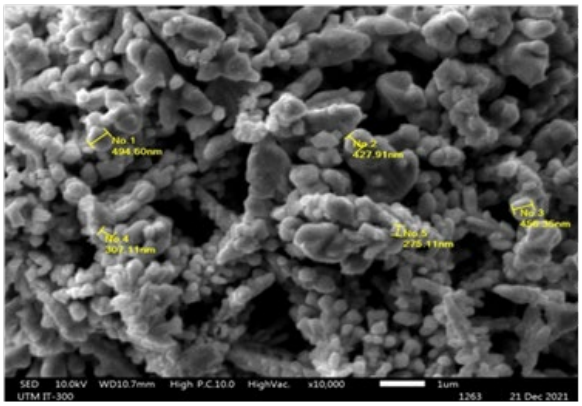

(b)

Element	Weight %	Weight % σ	Atomic %
Carbon	7.247	1.475	26.190
Aluminium	1.212	0.253	1.950
Chromium	16.921	0.752	14.127
Iron	67.541	1.486	52.499
Nickel	7.079	0.980	5.234

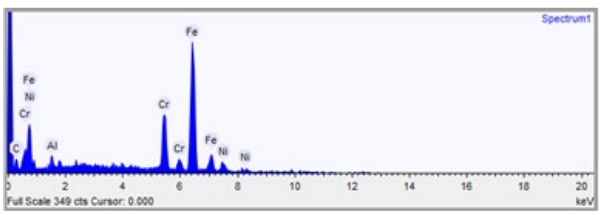

Figure 3. (a) Morphology image of Cu powder under SEM as viewed from the magnification of 10,000x and (b) EDX spectra of 304 SS after laser surface alloying

Figure 4 shows the images of the surface morphology of the alloyed track a magnification of 70x with a working voltage of 10.0 kV. At the speed of 0.4132 mm/s, there is no formation of pores produced, but rather the creation of holes as observed at 70W and 80W. With a slower scan speed, the interaction time between laser and material is high and greater energy density was supplied onto the material. The peak temperature increases substantially leading to an increased temperature gradient, thus inducing a stronger Marangoni fluid convection. Instead of melting the material, the laser was indenting it thus leading to the creation of holes. Increased surface tension and more dominant radial convection were the results of a greater temperature gradient created in the melt pool by a higher laser power. Consequently, it is observed that discernible pores appear at the maximum scanning speed of 0.6329 mm/s as marked in red circle The formation of these pores might happen due to lower laser-material interaction time resulting in the unfusion of powder and substrate as the energy density was not enough to melt the corresponding area of interest, thus leading to porosity. These pores would affect the mechanical bond of the samples, thus reducing the overall strength and inducing cracks. At 80W, a higher surface temperature was reached thus inducing a higher surface tension. This phenomenon creates gas entrapment due to Marangoni convection. Changes in surface tension influenced the behavior of gas bubbles within the melt pool, affecting their ability to coalesce and escape. Increased surface tension may also hinder the release of gas bubbles, leading to their accumulation and the formation of larger pores in the final microstructure. The size of the deposited track appeared larger when higher laser power was used alongside because of the higher energy density supplied onto the sample, thus inducing a higher heat dissipation which in return will increase the geometry of the melt pool. The most optimum deposited track can be observed at power 80W and a scanning speed of 0.4950 mm/s.

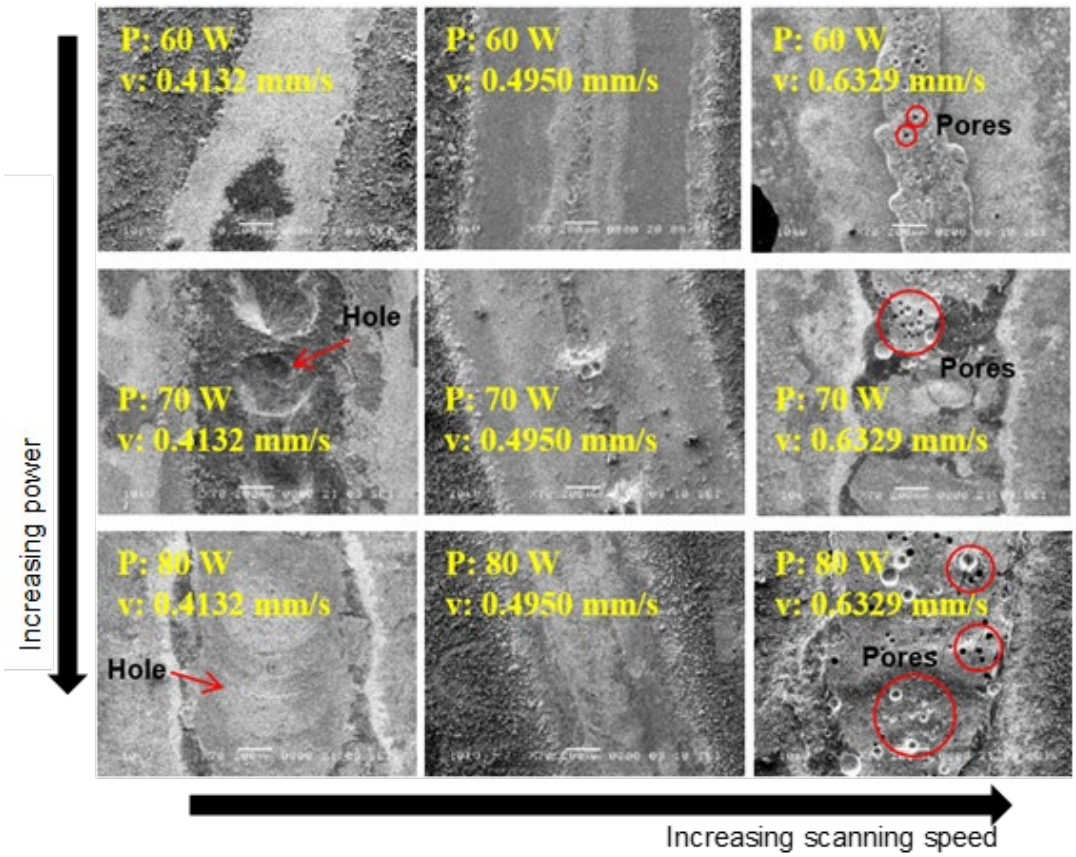

Figure 4. Surface morphology of the deposited track with respect to varying laser power and scanning speed

Microstructure properties of the melt pool was studied by varying the scanning speed of the process at 0.4132 mm/s, 0.4950 mm/s and 0.6329 mm/s respectively while keeping the laser power at constant value of 80 W. Figure 5 represents the microstructures at the alloyed zone with laser power at 80 W at different scanning speed; (a) 0.4132 mm/s, (b) 0.4950 mm/s, and (c) 0.6329 mm/s respectively. At the

lowest scanning speed of 0.4132 mm/s, the columnar grain size is on the average of 15-20 μm and a coarse microstructure was produced. Conversely, at the highest scanning speed of 0.6329 mm/s, the columnar grain size is on the average of 5-8 μm and a finer microstructure was produced. Higher scanning speeds result in shorter interaction times between the laser beam and the material, leading to faster cooling rates. With rapid cooling, the molten material solidifies more quickly, allowing less time for grain growth. This rapid solidification promotes the formation of finer grains in the microstructure.

The relationship of scanning velocity and solidification rate can be further verified by referring to equation:

$$R = v \sin \theta$$

where θ is the angle between the scanning direction and the growth vector's tangent, v is the scanning velocity, and R is the solidification rate. From the equation, the solidification rate is inversely proportional to the scanning speed. Based on the observation, it can be concluded that the sample's microstructure improves with increasing scanning speed. Higher scanning speeds correspond to higher solidification rates due to quicker cooling. This accelerated solidification process favors the formation of finer grains, as there is less time for grain coarsening to occur. The Marangoni effect, driven by temperature gradients within the melt pool, influences material flow and mixing during solidification. Higher scanning speeds result in more pronounced temperature gradients, which intensify the Marangoni-driven fluid flow. This enhanced mixing facilitates the distribution of alloying elements and promotes a more homogeneous microstructure with finer grains.

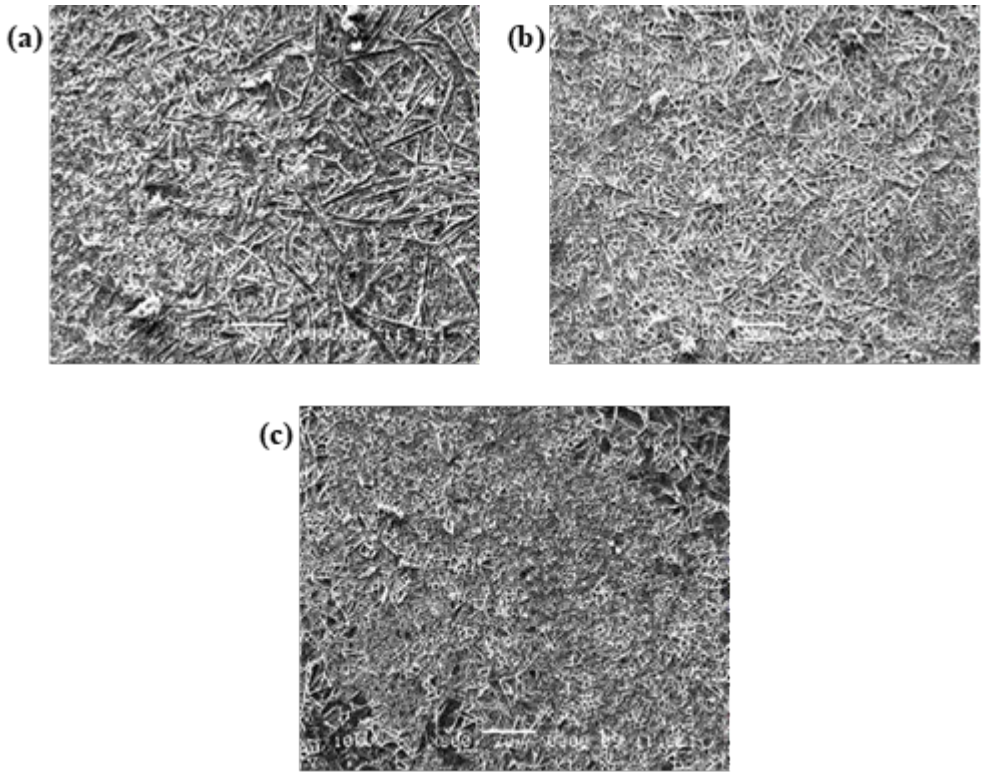

Figure 5. Microstructures at the alloyed zone with laser power at 80 W at different scanning speeds; (a) 0.4132 mm/s, (b) 0.4950 mm/s, (c) 0.6329 mm/s

The investigation on effect of varying laser power and scanning speed on the micro hardness of the melt pool has been conducted successfully. Microhardness profiles with varying laser power and laser scanning speed is presented in Figure 6 (a) and (b) respectively.

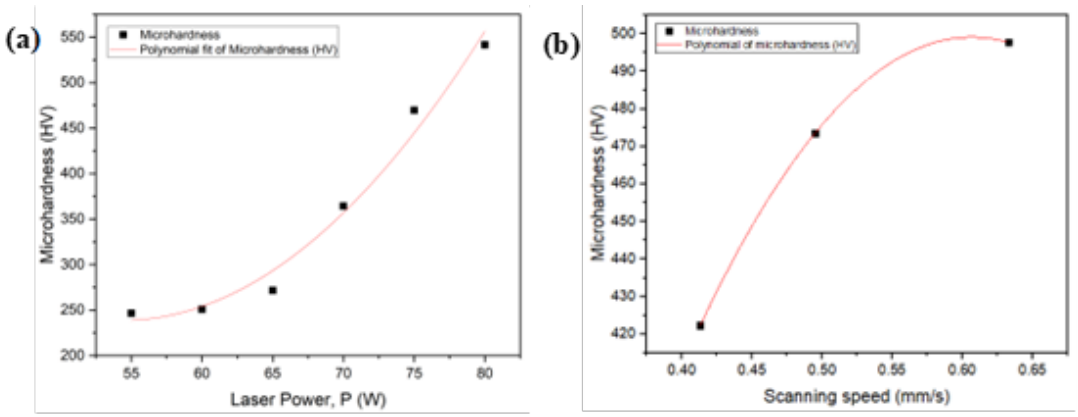

Figure 6. Microhardness profile across varying (a) laser power and (b) laser scanning speed

In Figure 6(a), it is observed that microhardness experiences an exponential increase with escalating laser power. As laser power is increased, more energy is delivered to the surface of the material. This higher energy density leads to more efficient melting and mixing of the alloying elements with the base material. The increased energy input promotes deeper penetration of the laser beam into the material, facilitating thorough alloying and homogenization of the surface composition. Consequently, the resulting alloyed surface tends to exhibit improved mechanical properties, including enhanced microhardness. The Marangoni effect, induced by temperature gradients within the molten pool, can also play a role in the observed increase in microhardness with escalating laser power. Higher laser power levels generate more pronounced temperature gradients, leading to enhanced material flow and mixing driven by surface tension gradients. This can result in more uniform distribution of alloying elements and refinement of the microstructure, contributing to improved mechanical properties, including microhardness.

By referring to Figure 6(b), an inverse exponential relationship between microhardness and scanning speed is evident. In laser surface alloying, scanning speed affects the duration of laser-material interaction and, consequently, the cooling rate during solidification. Higher scanning speeds result in shorter interaction times, leading to rapid cooling of the molten pool. This rapid cooling promotes the formation of a finer-grained microstructure due to limited time for grain growth. A finer grain structure typically enhances material properties such as microhardness. The Marangoni effect, driven by temperature gradients within the molten pool, can also influence microhardness variations with scanning speed. Lower scanning speeds result in longer residence times of the laser beam on the material surface, leading to more pronounced temperature gradients and, consequently, enhanced Marangoni-driven material mixing. This can promote more uniform distribution of alloying elements and refinement of the microstructure, potentially leading to improvements in microhardness.

The correlation between cooling time and grain size on the alloyed surface is pivotal, as it significantly impacts the subsequent microhardness value. A shorter cooling time typically leads to finer grain sizes, fostering increased microhardness due to a higher density of nucleation sites. Conversely, longer cooling times tend to yield coarser grain structures, often associated with lower microhardness values. In essence, the cooling rate during alloy solidification plays a decisive role in shaping the microstructure, consequently influencing the resulting microhardness.

Conclusion

In conclusion, experimenting with various combinations of laser power and scanning speeds for surface alloying offers a fresh approach. The investigation of the effect on melt pool dynamics, particularly the creation of holes and pores driven by Marangoni convection, is a significant contribution to the field. Based on the scope of the project, the experiment demonstrated that the sample achieved optimal quality for the deposited track when using a laser power of 80 W and a scanning speed of 0.4950 mm/s, showing no holes or pores. Additionally, the microstructure analysis of the melt pool revealed the formation of the finest grains when the scanning speed was highest, at 0.6329 mm/s. Moreover, the highest scanning speed also resulted in the highest microhardness, measured at 497.7 HV. This observation highlights the rapid cooling and solidification process within the melt pool, showcasing the unique and valuable findings of this research.

Conflict of Interest

The authors declare that there is no conflict of interest regarding the publication of this paper.

Acknowledgement

This research was supported by Universiti Teknologi Malaysia through UTM RA Iconic Grant (Q.J130000.4354.09G60) and UTM Fundamental Research (Q.J130000.3809.22H43).

References

[1] Montealegre, M., Castro, G., Rey, P., Arias, J., Vázquez, P., & González, M. (2010). Surface treatments by laser technology. *Contemporary Materials, 1*(1), 19–30.
[2] Hirose, A., & Kobayashi, K. F. (1994). Surface alloying of copper with chromium by CO2 laser. *Materials Science and Engineering: A, 174*(2), 199–206.
[3] Siddiqui, A. A., & Dubey, A. K. (2021). Recent trends in laser cladding and surface alloying. *Optics & Laser Technology, 134*, 106619.
[4] Chi, Y., Gu, G., Yu, H., & Chen, C. (2018). Laser surface alloying on aluminum and its alloys: A review. *Optics and Lasers in Engineering, 100*, 23–37.
[5] Majumdar, J. D., & Manna, I. (2010). Mechanical properties of a laser-surface-alloyed magnesium-based alloy (AZ91) with nickel. *Scripta Materialia, 62*(8), 579–581.
[6] Xu, G., Li, P., Cao, Q., Hu, Q., Gu, X., & Du, B. (2018). Modelling of fluid flow phenomenon in laser+ GMAW hybrid welding of aluminum alloy considering three phase coupling and arc plasma shear stress. *Optics & Laser Technology, 100*, 244–255.
[7] Lei, Z., Wu, S., Li, P., Li, B., Lu, N., & Hu, X. (2019). Numerical study of thermal fluid dynamics in laser welding of Al alloy with powder feeding. *Applied Thermal Engineering, 151*, 394–405.
[8] Shi, L., Jiang, L., & Gao, M. (2022). Numerical research on melt pool dynamics of oscillating laser-arc hybrid welding. *International Journal of Heat and Mass Transfer, 185*, 122421.
[9] Xiao, X., Lu, C., Fu, Y., Ye, X., & Song, L. (2021). Progress on experimental study of melt pool flow dynamics in laser material processing. In *Liquid Metals* (pp. 1–15). IntechOpen.
[10] Mahmood, M. A., Ur Rehman, A., Pitir, F., Salamci, M. U., & Mihailescu, I. N. (2021). Laser melting deposition additive manufacturing of Ti6Al4V biomedical alloy: Mesoscopic in-situ flow field mapping via computational fluid dynamics and analytical modelling with empirical testing. *Materials, 14*(24), 7749.
[11] Dai, D., Gu, D., Ge, Q., Ma, C., Shi, X., & Zhang, H. (2020). Thermodynamics of molten pool predicted by computational fluid dynamics in selective laser melting of Ti6Al4V: Surface morphology evolution and densification behavior. *Computer Modeling in Engineering & Sciences, 124*(3), 1085–1098.
[12] Ur Rehman, A., Mahmood, M. A., Pitir, F., Salamci, M. U., Popescu, A. C., & Mihailescu, I. N. (2021). Mesoscopic computational fluid dynamics modelling for the laser-melting deposition of AISI 304 stainless steel single tracks with experimental correlation: A novel study. *Metals, 11*(10), 1569.
[13] Wang, C., Han, J., Zhao, J., Song, Y., Man, J., Zhu, H., Sun, J., & Fang, L. (2019). Enhanced wear resistance of 316 L stainless steel with a nanostructured surface layer prepared by ultrasonic surface rolling. *Coatings, 9*(4), 276.
[14] Zhang, G., Liu, H., Tian, X., Chen, P., Yang, H., & Hao, J. (2020). Microstructure and properties of AlCoCrFeNiSi high-entropy alloy coating on AISI 304 stainless steel by laser cladding. *Journal of Materials Engineering and Performance, 29*, 278–288.
[15] Li, D., Wu, J., Miao, B., Zhao, X., Mao, C., Wei, W., & Hu, J. (2020). Enhancement of wear resistance by sand blasting-assisted rapid plasma nitriding for 304 austenitic stainless steel. *Surface Engineering, 36*(5), 524–530.
[16] Rotshtein, V. P., Ivanov, Y. F., Markov, A. B., Proskurovsky, D. I., Karlik, K. V., Oskomov, K. V., Uglov, B. V., Kuleshov, A. K., Novitskaya, M. V., Dub, S. N., & Pauleau, Y. (2006). Surface alloying of stainless steel 316 with copper using pulsed electron-beam melting of film–substrate system. *Surface and Coatings Technology, 200*(22–23), 6378–6383.
[17] Rafiei, M., & Mostaan, H. (2019). The effect of filler metal and butter layer on microstructural and mechanical properties of pure Cu to AISI304 stainless steel dissimilar joint. *Proceedings of the Institution of Mechanical Engineers, Part L: Journal of Materials: Design and Applications, 233*(9), 1894–1905.
[18] Sutton, A. T., Kriewall, C. S., Karnati, S., Leu, M. C., & Newkirk, J. W. (2020). Characterization of AISI 304L stainless steel powder recycled in the laser powder-bed fusion process. *Additive Manufacturing, 32*, 100981.
[19] Sun, S., Brandt, M., & Easton, M. (2017). Powder bed fusion processes: An overview. In *Laser Additive Manufacturing* (pp. 55–77).